Position controller for a flapping-wing drone using UWB

Guillermo González*, Guido C.H.E de Croon, Diana Olejnik and Matěj Karásek
Delft University of Technology, Mekelweg 5, Delft

ABSTRACT

This paper proposes an integral approach for accurate ultra wide band indoor position control of flapping wing micro air vehicles. Three aspects are considered to reach a reliable and accurate position controller. The first aspect is a velocity/attitude flapping-wing model for drag compensation. The model is compared with real flight data and shown to be applicable for more than one type of flapping wing drone. The second improvement regards a battery-level dependent thrust control. Lastly a characterisation of ground effects in flapping-wing flight is obtained from hovering experiments. The proposed controller improves position control by a factor $\sim$ 1.5, reaching a mean absolute error of 10cm for position in x and y, and 4.9cm for position in z.

1 INTRODUCTION

The fact that drones are becoming increasingly popular is intimately related with the development of more sophisticated automation resources. In the case of drones, weight, processing speed, and energy consumption are critical aspects to accomplish fully autonomous flights. Therefore, elements such as motors, micro-processors, memory units and batteries need to be continuously improved to meet these requirements. These conditions have fostered the development of flapping wing micro-air vehicles (FWMAV). This type of UAV is inspired on the flight of birds and insects, and has become attractive in the field of small-scale micro-air vehicles, since it provides both the ability of hovering and flying into any direction. After the foundational work from Ellington [1] and Dickinson [2], many experiments have been carried out in order to get an optimal physical design of FWMAVs, as well as velocity and position controllers to keep a stable flight.

Regarding position feedback, the most common option is an indoor positioning system (IPS). Some of the technologies used for for IPS are Wi-fi, Radio Frequency Identification (RFID), and infrared (IR) motion tracking systems. Wi-fi and RFID can be found for tracking mobile devices, but not specifically for drones [3]. IR is used for indoor tracking of drones (e.g. VICON/OptiTrack), but it is an expensive option and its accuracy can be affected by lighting conditions [4].

Another option for IPS is ultra wide band (UWB) which was already defined in 2006, but just recently started to gain popularity. UWB is able to transmit in nano-second scale periods. Thus it allows excellent timing for signal arriving, which translates to centimeter level accuracy. Its low spectral density reduces the interference with other RF devices. However, it also has some drawbacks like high computational and memory capacity of the controller and its vulnerability to multi-path effect when signals bounce with the physical boundaries of the environment [5].

Inertial navigation systems (INS) are usually added in indoor environments to complement IPS. Usually INS systems employ micro-electro mechanical systems (MEMS) or inertial measurement units (IMU). Furthermore, data fusion is also applied for better accuracy, by means of a Kalman filter. Hence many combinations of integrated systems have been proposed. For example a GPS/UWB/MEMS navigation system with Kalman filter [6] and INS/UWB system based on a fuzzy adaptive Kalman filter [7]. Although most of these implementations provide a basis for designing an autonomous position controller, it is important to keep in mind they are specifically designed either for fixed-wing or quadrotor UAVs. In the case of flapping wing drones some extra constraints shall be considered like the physical limitations in terms of payload and energy consumption, or the noise influence in IMU measurements due to high frequency mechanical vibration [8]. To overcome these circumstances, the existing solutions must be adapted, leaving a potential research development for position controllers of FWMAVs.

One of the challenges of working with FWMAVs comes from the aerodynamics of the system. A reliable model of the dynamics can significantly increase the performance and accuracy. Nevertheless, most aerodynamic models for flapping wings require extensive system identification techniques for numerous parameters, whose values only remain valid for a specific drone. A widespread alternative is the use of quasi-steady models where force coefficients are obtained either from experimental data or from theoretical principles [9]. The control strategy proposed in this paper follows a simpler solution where the model is obtained by directly averaging aerodynamic parameters as functions in terms of the body velocities. Albeit the method may be considered just a rough approximation compared to quasi-steady models, it tends to be more practical since just a reduced amount of parameters is required. When validating averaging parameters with real flight data, several authors address the issues of un-

*Email address(es): g.gonzalezarchundia@student.tudelft.nl,
g.c.h.e.decroon@tudelft.nl,
d.a.olejnik@tudelft.nl,
matej@flapper-drones.com

steady flight due to mechanical vibrations [10, 11]. However just some models follow an approach based on drag compensation. Within the few cases where drag compensation models are implemented, most of them are linear models, which are only valid for a limited range of velocities [8, 12].

Similar to most MAVs, FWMAVs are also prone to short flights due to the limited size of the batteries they are able to carry. Thus it is common that voltage will significantly change during flight, affecting as well the required throttle level for hovering [13]. This condition poses a challenge in height control, for both reaching and keeping a specific position along the z axis.

Another issue affecting height control is the ground effect. This phenomenon particularly occurs when the drone is flying close to the ground [14]. An extra thrust is generated because the wind currents underneath the drone bounce against the ground, causing the drone to behave like sitting on a cushion of air [15]. Thus, an extra lift is generated, causing the output thrust to be higher than the input thrust.

This paper addresses the three aforementioned challenges of FWMAVs. Sections 2, 3 and 4 provide the background for the implementation. Section 5 describes how averaging parameters are applied for drag compensation. Section 6 discusses the issues of changing voltage and ground effects. Lastly, Section 7 shows the results on how the transient response is improved in any of the three axes: forward (x-axis), sideways (y-axis) and vertical (z-axis).

2 EXPERIMENTAL SETUP

Since the work on this project relies mainly on feedback through UWB, the experimental setting should be a grid where UWB receivers are strategically located in the vertices and the transceiver is mounted on the FWMAV. This way, the drone flies inside the volume of a cube bounded by the position of the anchors. A similar set-up is used in [16], where the eight anchors on the corners optimise the possibility for the drone to have line-of-sight at least with one anchor. Such a grid was set-up at the Cyberzoo (shown in Figure 1), the flight arena of the TU Delft Faculty of Aerospace, which is known as the main facility of the university for performing tests on drones, and has a size of $10m \times 10m \times 7m$. A reliable choice for UWB sensor is the Decawave DWM1000, as it has proven to give successful results for UAV tracking [17]. The UWB sensors are used as the anchors of the IPS and are set to work using a time difference of arrival (TDOA) algorithm.

In order to have a reference for the UWB measurements, a motion tracking system is used for measurements of position and rotations. It consists of 12 OptiTrack Prime 17W motion tracking cameras (set to resolution 1664 px $\times$ 1088 px, 50 fps) and has proven to deliver accurate results for MAV test flights [18]. When working with the motion tracking system, the drone was equipped with four retro-reflective markers placed on the landing gear of the drone, and the UWB sensor was placed at the top to optimise direct line of sight

Figure 1: Cyberzoo structure where the UWB anchors are placed (left) and detail of UWB anchor mounted on the structure (right)

(Figure 2).

About the flapping-wing drone, referred in this paper as Flapper, is a design from the company Flapper-drones [19]. It is a 102g tailless FWMAV with a wingspan of 49cm, able to keep flapping frequencies up to 12 Hz when hovering. The on-board processing hardware consists of a Crazyflie Bolt autopilot board, including an IMU with 3-axis accelerometer/gyroscope (BMI088). The data link between the autopilot and the ground station is done with a Crazyradio PA (also from Bitcraze), which is a USB radio dongle based on nRF24LU1+ from Nordic Semiconductor. The system can be powered with a 300-mAh two-cell 7.4V LiPo battery, reaching a flight time between 4-6 minutes, depending on the internal resistance of the battery.

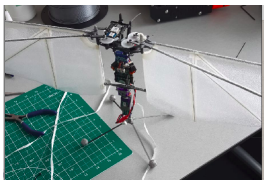

Figure 2: Flapper drone equipped with IR markers and UWB sensor

3 CONTROL LOOP

For autonomous flight, the flapping-wing drone uses a cascaded PID-controller, based on the structure presented by [20]. The controller consists of three loops. The output provides the control signals for the motors involved in the flight dynamics of the drone: two brush-less motors in charge of the flapping frequency for thrust and roll, one servo-motor that modifies the angle of the dihedral for pitch, and another servo-motor that changes the deflection of the wings for yaw.

Regarding the structure of the cascaded loops, the innermost loop is in charge of attitude rate and runs at 500Hz. The intermediate loop also runs at 500Hz and is in charge of attitude control. The outer loop is the position/velocity control, which runs at 100Hz and can take either position or velocity commands.

Another remark is the trimming values for servos in charge of pitch, roll and yaw. This procedure must be done in order to get the proper behaviour from the controller. For

trimming, one should fly the drone manually until it hovers at a steady position. The trim values are the pitch, roll and yaw commands given to keep the drone hovering. The values are specific for each flapping-wing drone, as they change depending on manufacturing factors. Thus it is important to properly set the appropriate trimming values before going further with any flight test.

4 STATE ESTIMATION

The state estimation is done by means of an Extended Kalman Filter (EKF) which fuses the measurements of the IMU and the UWB positioning system. The model of the EKF is the same as the one proposed by [21], which considers a nine-dimensional state vector defined as:

$$S = \begin{bmatrix} x_E & v_B & d \end{bmatrix}^T \tag{1}$$

Where x_E is the position vector in global frame, v_B is the velocity vector in body frame and d is an attitude error vector, where the error is defined as the difference between the last measured attitude and the current attitude. The purpose for using attitude errors instead of the conventional Euler angles is to simplify the state prediction equations because it only considers the increments in roll, pitch and yaw. A more detailed explanation on the implementation of the filter is given in [21].

The main advantage of fusing UWB with IMU through the Kalman filter is the attitude correction to account for the drift in pitch and roll caused by sensor noise and bias. For instance, when the Flapper is left standing up, the Kalman filter resets correctly the roll and pitch to zero when UWB measurement are coming in. On the other side, a complementary filter, which relies only on IMU data, will converge to a certain drift and thus propagates it through time.

One last adjustment done to the EKF aims to diminish the detrimental effects on position estimation caused by multipath UWB signals. Specially when going close to the ground, the position estimates tend to drift for more than 20 cm. A way to account for the wrong measurements when flying close to the ground is to use a variable sensor noise value R_{uwb} for measurements from UWB, rather than a constant value. Consequently, the sensor noise is defined as:

$$R_{uwb} = \lambda(\hat{z})\sigma^2_{uwb} \tag{2}$$

Where $\lambda(\hat{z})$ is a factor dependent on the estimated height $\hat{z}$, in meters. For the implementation, $\lambda = 0.5$, for $z \geq 1$; $\lambda = 1.5 - \hat{z}$, for $0.5 < \hat{z} < 1$; and $\lambda = 1$, for $z \leq 0.5$. The effect of variable sensor noise in position estimation was tested by placing the drone static on the ground, at the origin (0,0,0) of the UWB IPS. The plots from Figure 3 show the estimated position (est) in contrast to the real position (cmd), Both values were sampled at 50Hz, during 8 seconds. Using the variable sensor noise R_{uwb} significantly increases the accuracy in estimation approximately by 0.2m in the three axes.

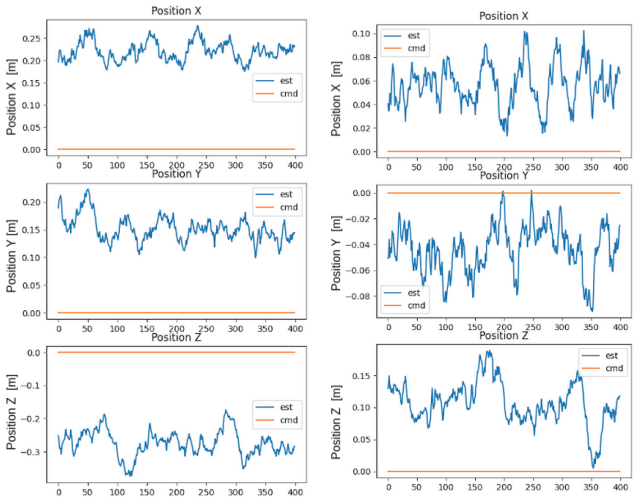

Figure 3: Effects in position estimation before using variable sensor noise (left) and after implementing it (right).

Once the variable sensor noise term was implemented into the EKF, several flight paths were tested (linear, square, rhombus and hexagonal paths). The measurements from UWB using a TDOA algorithm proved to be reliable enough for position estimation. The mean absolute error obtained in all cases remained between 8-10 cm, when compared to the measurements from the Optitrack system.

5 DRAG COMPENSATION

The first technique for yielding a better control strategy for FWMAVs was to obtain a model for drag compensation. Since the drag is typically neglected in aerodynamic models, there tends to be an offset between the commanded velocity and the velocity output by the controller. Usually a feed forward term is used to compensate for these drag effects. Following the structure of the controller in Section 3, the velocity loops provides the input for the attitude loop. Thus, feed forward is modelled as a function of velocity:

$$\theta_{FF} = f(v_{xE}) \tag{3}$$

$$\varphi_{FF} = f(v_{yE}) \tag{4}$$

Where Eq. (3) is the feed forward term for pitch and Eq. (4) is for roll. In order to derive such a model, a system identification experiment is proposed based on the supplementary materials from [22], where step inputs in roll and pitch are given to the flapping-wing drone and then the transient response is recorded. The experiments are done using manual flight via a Frsky RC-controller where the pitch and roll step inputs are pre-programmed. The tracking data is recorded with the motion tracking system mentioned in Section 2.

Figure 4 is given as an example of the transient response in velocity obtained for different step-inputs in pitch (a similar response is obtained for roll angles). Due to limitations

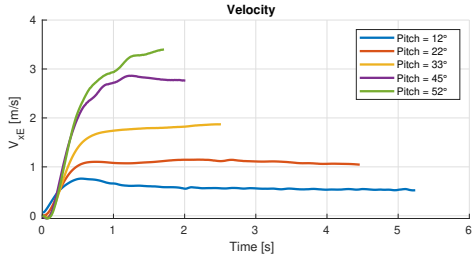

Figure 4: Velocities attained at different pitch step inputs

on the size of the flight arena, only for the small angles (below 45°) it is possible to reach the steady-state velocities. For higher angles, a common technique to reach the steady-state velocities is to perform wind-tunnel experiments [23]. In this case, an alternative method is used where a non-linear regression model is obtained for the smaller angles and then it is used to extrapolate the data at higher angles. From figure 4, it can be appreciated that the transient response approximates to the behaviour of a first-order system. Hence, the equation for the transient response is modelled as an exponential function of the form:

$$v(t) = a - be^{-ct+d} \tag{5}$$

The parameters a, b, c and d from Eq. (5) have to be initialised with certain values, depending on the shape of the curve obtained from the measured data points. The final steady-state values obtained from the extrapolation model strongly depend on how many data points are considered for the regression model. Hence, Table 1 shows the absolute error between the last measured velocity for each angle, and the respective value calculated from the extrapolation model. For the angles of 30° or less, this velocity approximates to the steady-state velocity. For angles of 45° or above, the last measured velocity is used as ground truth equilibrium velocity, although it is still part of the transient response.

Final velocity error at different pitch angles [m/s]					
Data taken for regression	**12°**	**22°**	**33°**	**45°***	**52°***
10%	0.124	0.0752	0.1842	0.2641	0.276
30%	0.0318	0.0459	0.0347	0.1899	0.1259
50%	0.0166	0.0636	0.015	0.2048	0.0038
70%	0.0183	0.0632	0.0282	0.1379	0.0402
90%	0.0142	0.0561	0.0289	0.0857	0.0185
Final velocity error at different roll angles [m/s]					
Data taken for regression	**12°**	**22°**	**33°**	**47°***	**52°***
10%	0.1007	0.1479	0.0391	0.2972	0.3028
30%	0.10	0.1216	0.0452	0.2303	0.2366
50%	0.0262	0.1427	0.0325	0.0499	0.0849
70%	0.0234	0.0802	0.0378	0.0486	0.095
90%	0.0268	0.0247	0.0261	0.0266	0.0757

Table 1: Extrapolation errors taking different amounts of data for regression model. *Indicates that for those angles the final velocity is not considered as ground truth. Hence these errors are overestimated.

As expected, results from Table 1 show on the angles of accurate ground truth (12º,22º and 33º) that the overall accuracy of the extrapolation model, for both pitch and roll, increases as more data points are taken for the regression. Individually, for each angle, accuracy remains approximately the same with 50% of the data points or more. For illustration purposes, Figure 5 shows the predicted steady-state velocity for each angle when taking 70% of the data points for the regression model. Nevertheless, the real steady-state values used were the ones obtained taking all of the data points since those ones result in the lowest error.

Once the steady-state velocity for each angle is available, the pitch-velocity and roll-velocity models can be obtained. Given the mapping of the steady-state velocity/attitude pairs, different regression models were tested to approximate the relationship the models (linear, quadratic and exponential). Since the maximum roll and pitch angle is 90° for a FWMAV, it is expected that the velocity will converge to a maximum value as the angle approaches 90°. Thus, the model is approximated as the exponential function in Eq. (6). Linear or quadratic models could be used as well, but they would only be valid within specific ranges since they do not converge to a constant value.

$$v(\theta) = a + be^{-c\theta} \tag{6}$$

Using the obtained steady-state velocity, a nonlinear regression model is obtained using Eq. (6). For both pitch and roll the parameters are initialised as: $a = -90, b = 90$ and $c = 0.3$. Moreover, to test the applicability of the exponential model, the same described procedure was applied to the data sets from [22] regarding the Delfly Nimble (a 33cm-wingspan FWMAV of the same type). Then the nonlinear regression model is applied initialising the parameters with exactly the same values. Figure 6 shows how the exponential curves of the Flapper and the Delfly properly approximate to the given data points for both roll and pitch.

6 HEIGHT CONTROL

Having a reliable height control strategy is essential to guarantee successful autonomous flight. Mainly it is used to keep the drone flying at a certain altitude and for hovering. Nevertheless, it also plays a major role in landing, which is known to be as the most challenging phase of flight for any aircraft. Height control is intimately related with thrust. Therefore, two approaches for improving thrust command were considered, first one is a voltage-dependent thrust model, and second one is an analysis of the ground effects.

6.1 Voltage-thrust model

Thrust is part of the position and velocity control of the drone, it also involves a PID controller which takes a commanded throttle and delivers an output signal for the motors. The signal from the controller is summed with a feed forward

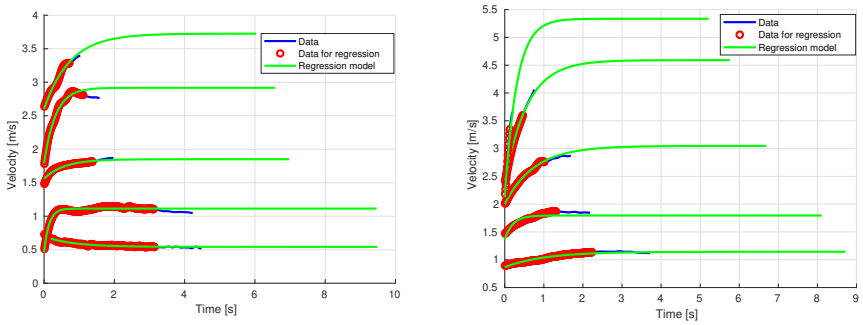

Figure 5: Extrapolation models for pitch (left) and roll (right) at different velocities

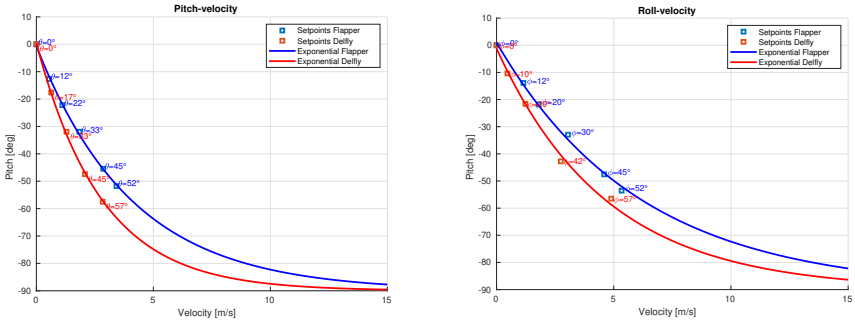

Figure 6: Pitch/velocity (left) and roll/velocity(right) models obtained from extrapolated data

term known as base thrust, which is the thrust required to keep the drone hovering at a certain altitude. In most cases the base thrust is a constant value, but there is evidence that the required base thrust tends to increase as the battery voltage drops off [13]. In order to observe this behaviour, a series of experiments were done where the drone started flying with a fully-charged battery and then let it hover until the battery got discharged. all values were sampled at 50 Hz and mapped as depicted in Figure 7.

Throttle is used instead of thrust because this is the signal that is directly input into the motors. In this case, throttle is a dimensionless value where 30000 sets the motors to the lowest speed and 60000 indicates full speed. The data points are then filtered and used to create a regression model. The improvement when increasing the order of the regression model is not significant. First, second and third-order models yield $R^2 \approx 0.756$. Albeit there is noisy data involved, it is not considered for the regression model since it is already known that the noise comes mainly from the feedback of the controller and the IMU measurements. Nevertheless, there is the option of using alternative regression models to account for the stochastic behaviour observed in Figure 7, which may result in a better R^2 value.

Once the model is implemented, the base thrust turns into a variable base thrust whose value will tend to increase the longer the drone keeps flying. To evaluate the model, a series of experiments was conducted using four different thrust controllers: a P and PI height controller, using both the constant and variable base thrust. For each controller, the flight was analysed in five different directions: X-motion, Y-motion, Z-motion, XZ-motion and YZ-motion. For each motion, a flight test was done consisting on five repetitions of step-input commands in the given motion, in order to get an average behaviour. Hence, Table 2 summarises the standard deviation and the mean absolute error between the transient response and the commanded height for each motion and controller. Notice from the table that for most of the motions, using a PI will result in lower error than a P controller, regardless of the

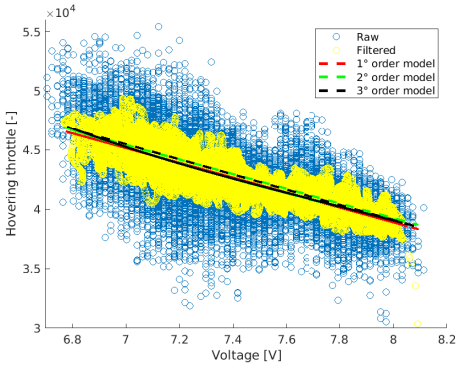

Figure 7: Throttle and voltage mapping with tendency lines for different regression models

variable or constant base thrust. For most conditions, variable PI reaches the lowest mean absolute error and standard deviation, showing the utility of varying thrust model.

Figure 8 depicts the averaged transient response in height for each controller, for the cases of X motion and XZ motion. The reduction of steady-state error caused by the integral gain is clear in the X motion, where the drone should keep flying at the same height when moving from one position to another. The XZ motion shows a case in which variable thrust model performs less well. In motions where a change in height occur, performance is more similar between P and PI controllers. From one side the integral gain tends to increase the settling time compared to the P controller, but at the same time the oscillations of the PI response reduces the error to minimum whenever it crosses the commanded value.

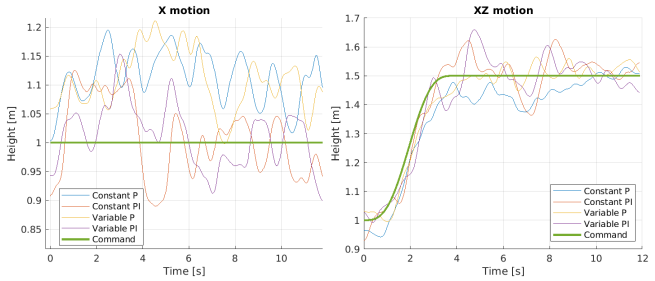

Figure 8: Extrapolation models for pitch (left) and roll (right) at different velocities

6.2 *Ground effect*

For the second approach in height control, the target was to investigate whether the ground effect has a large effect when flying low. According to [14], the range of height in which ground effects usually occur is $3d > h > d$, where d is the diameter of propellers in quadrotors. Similarly, for a FWMAV, the range would be proportional to the wingspan (0.5m). Hence, the experiments to model the ground effect consisted on keeping the drone hovering at different heights between 0.33m and 1.2m for over a minute. The lowest height tested was 0.33m above the ground, since this was the lowest height at which the drone can be kept hovering autonomously due to the location of the UWB anchors. In this section, the height is considered to be the distance between the landing gear and the ground. For each different height, a mean thrust and mean voltage is obtained. Using the thrust-voltage relationship found previously, the corrected thrust can be obtained. The ratio between the corrected thrust and the mean thrust is specific for each different height, as depicted in figure 9. Notice that for each data point an upper and lower bound is also provided based on the standard deviation of the thrust and battery voltage. According to [24], the relationship between thrust ratio and height can be modelled as:

$$\frac{T_{input}}{T_{output}} = 1 - \lambda \left(\frac{1}{h-a} \right)^2 \tag{7}$$

After mapping the thrust ratio with their respective height, a non-linear regression model using equation Eq. (7) is applied. Such model approximates the coefficients $\lambda = 0.00093$ and $a = 0.4213$. In Figure 9, the regression model stays within the bounds of each data point. At the tested heights the ground effect still has relatively little influence on the thrust ratio. The thrust ratio only decreases to 92% at the lowest height of 0.33m. Thus, the ground effect is little up to 0.33m. Lower heights are not considered relevant, because, due to the disposition the UWB anchors, the drone is unlikely to fly lower except during take-off and landing. Nevertheless, the fit shows a sharp drop-off below 0.33m. Whether this is correct will have to be confirmed with future experiments.

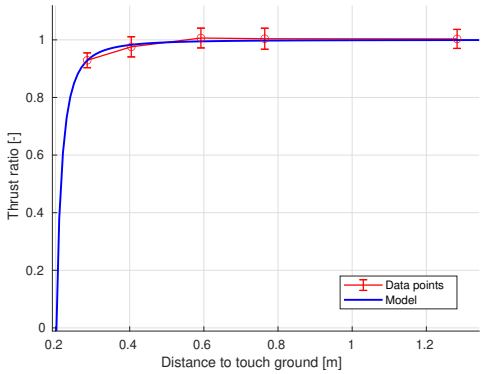

Figure 9: Thrust ratio for each height

.

7 EXPERIMENTAL VALIDATION

Once all the modifications were done, two versions of the controller were tested for validation. The first version is referred as "raw" version, which is the working implementation with the default EKF and PID controller mentioned in Section 3, without the proposed enhancements. The second version is referred as the "modified" version, and is the implementation with the adaptations mentioned in Sections 4, 5, and 6.

The validation consists of analysing the transient responses in position and velocity when position step-inputs were given in x, y, and z. For a wider perspective on the stability of the controller, the amplitude of the step input was changed from 1m to 2m. Thus, any difference in the aggressiveness of the response can be detected as well. For each motion and step-input, a series of five repetitions was done and averaged to obtain the general behaviour of the transient response. Table 3 presents how the mean absolute error, for both position and velocity, decreases when using the modified controller instead of the raw controller. In general, errors are approximately 1.5 times lower after the modifications.

	X motion		Y motion		Z motion		XZ motion		YZ motion		Overall	
Controller	Mean	Std. dev.	Mean	Std. dev.	Mean	Std. dev.	Mean	Std. dev.	Mean	Std. dev.	Mean	Std. dev.
Constant P	0.109	0.08	0.098	**0.075**	0.077	0.117	**0.035**	0.166	0.043	0.143	0.072	0.116
Constant PI	0.061	0.159	0.048	0.093	**0.06**	0.075	0.047	**0.09**	0.047	0.1175	0.053	0.107
Variable P	0.114	**0.069**	0.086	0.079	0.065	0.069	0.057	0.116	0.046	0.1038	0.074	0.09
Variable PI	**0.049**	0.107	**0.025**	0.083	**0.06**	**0.056**	0.05	0.092	**0.037**	**0.061**	**0.044**	**0.08**

Table 2: Errors and standard deviations for each controller. Best result for each condition is bold-cased.

Mean absolute error for position step input 1						
	X motion		**Y motion**		**Z motion**	
Version	Raw	Modified	Raw	Modified	Raw	Modified
Position [m]	0.1706	**0.105**	0.1898	**0.1048**	0.0496	**0.043**
Velocity [m/s]	0.3945	**0.1297**	0.3001	**0.1199**	0.1001	**0.0892**
Mean absolute error for position step input 2						
	X motion		**Y motion**		**Z motion**	
Version	Raw	Modified	Raw	Modified	Raw	Modified
Position [m]	0.3316	**0.1978**	0.2989	**0.2055**	0.1245	**0.1097**
Velocity [m/s]	0.6330	**0.2859**	0.4583	**0.1802**	0.2476	**0.1613**

Table 3: Mean absolute errors of validation experiments. Best performance for each case is bold-cased.

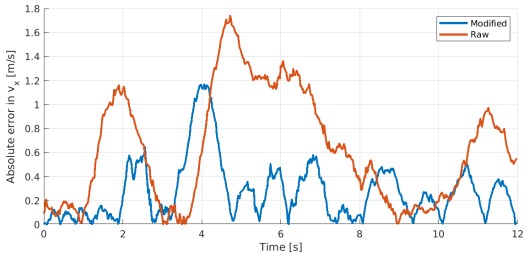

(a) Absolute error in Velocity X

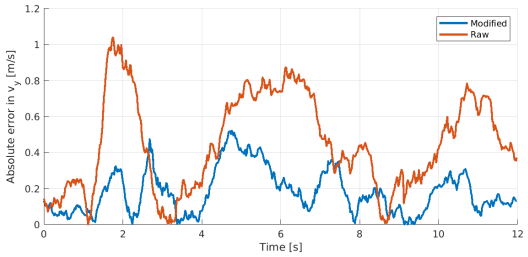

(b) Absolute error in Velocity Y

Figure 10: Comparison of velocity error during transient response to a step input of amplitude 2

Lastly, Figure 10 illustrates how the absolute error obtained in the transient response of the modified version is smaller and more consistent than the one of the raw version. For the sake of simplicity, only the transient responses of velocity in x and y to the step input of 2m are given, as the increase in performance in those two is the largest, according to Table 3. In Figure 10 the error is defined as the absolute difference between the output value and the corresponding commanded value. The plotted error corresponds to the transient response when the step input of amplitude 2 is given at $t = 1$s. Notice that almost throughout the whole response the error of the modified version is lower than the one of the raw version. Moreover, most of the peaks of the modified version are roughly 75% smaller than the ones from the raw version.

8 CONCLUSIONS

The achievement from this work was defining a strategy for enhancing position control for FWMAVs. From the estimation perspective, the strategy uses an extended Kalman filter to fuse UWB and IMU data, and it also incorporates a variable sensor noise term. Altogether, state estimation achieves accuracy between 8-10 cm error. From the control side, three specific aspects are considered.

Firstly, a velocity/attitude nonlinear model, which showed to be valid for two different kinds of FWMAVs. Thus, proving that it can be adapted, as long as there is experimental data from which the steady-state velocity can be extrapolated for a certain angle. Moreover, the model was validated using real flight data and proved its efficacy for drag compensation as part of the feed-forward term in the velocity control loop.

Secondly, the lower standard deviation of voltage-dependent thrust, compared to constant thrust, demonstrates a more consistent performance through time. A more notorious contrast can be obtained if the FWMAV flies for longer periods.

Thirdly, the ground effect experiments prove that as long as the drone's wings fly above 0.5m from the ground, no significant additional thrust will appear. Nevertheless, to know how much extra thrust is produced below 0.5m, experiments should be done through manual flight.

Lastly, in order to improve performance in autonomous flight using UWB, further development can be done in the position estimation. For instance drag is not considered in the EKF for the estimation of body velocities. An option would be deriving a drag model from IMU data. Other approach would be fusing data from other sources (e.g. barometer and magnetometer data) to compensate for the noisy accelerometer measurements due to inherent mechanical vibrations from flapping wing flight.

ACKNOWLEDGEMENTS

The realisation of this paper was possible thanks to the support of the start-up Flapper Drones B.V., and the MAVLab from the TU Delft Faculty of Aerospace.

REFERENCES

[1] Charles Porter Ellington. The aerodynamics of hovering insect flight. IV. Aerodynamic mechanisms. *Philosophical Transactions of the Royal Society of London. B, Biological Sciences*, 305(1122):79–113, 1984.

[2] Michael H Dickinson, Fritz-Olaf Lehmann, and Sanjay P Sane. Wing rotation and the aerodynamic basis of insect flight. *Science*, 284(5422):1954–1960, 1999.

[3] Juan J Pomárico-Franquiz, Moises Granados-Cruz, and Yuriy S Shmaliy. Self-localization over RFID tag grid excess channels using extended filtering techniques. *IEEE Journal of Selected Topics in Signal Processing*, 9(2):229–238, 2014.

[4] Abdulrahman Alarifi, AbdulMalik Al-Salman, Mansour Alsaleh, Ahmad Alnafessah, Suheer Al-Hadhrami, Mai A Al-Ammar, and Hend S Al-Khalifa. Ultra wideband indoor positioning technologies: Analysis and recent advances. *Sensors*, 16(5):707, 2016.

[5] Bardia Alavi and Kaveh Pahlavan. Modeling of the TOA-based distance measurement error using UWB indoor radio measurements. *IEEE Communications Letters*, 10(4):275–277, 2006.

[6] Zengke Li, Guobin Chang, Jingxiang Gao, Jian Wang, and Alberto Hernandez. GPS/UWB/MEMS-IMU tightly coupled navigation with improved robust kalman filter. *Advances in Space Research*, 58(11):2424–2434, 2016.

[7] Qigao Fan, Yaheng Wu, Jing Hui, Lei Wu, Zhenzhong Yu, and Lijuan Zhou. Integrated navigation fusion strategy of INS/UWB for indoor carrier attitude angle and position synchronous tracking. *The Scientific World Journal*, 2014, 2014.

[8] Karl Martin Kajak, Matej Karásek, Qi Ping Chu, and GCHE De Croon. A minimal longitudinal dynamic model of a tailless flapping wing robot for control design. *Bioinspiration & Biomimetics*, 14(4):046008, 2019.

[9] Mostafa RA Nabawy and William J Crowther. The role of the leading edge vortex in lift augmentation of steadily revolving wings: a change in perspective. *Journal of the Royal Society Interface*, 14(132):20170159, 2017.

[10] Dong Xue, Bifeng Song, Wenping Song, Wenqing Yang, Wenfu Xu, and Tao Wu. Computational simulation and free flight validation of body vibration of flapping-wing mav in forward flight. *Aerospace Science and Technology*, 95:105491, 2019.

[11] JL Verboom, Sjoerd Tijmons, Christophe De Wagter, B Remes, Robert Babuska, and Guido CHE de Croon. Attitude and altitude estimation and control on board a flapping wing micro air vehicle. In *2015 IEEE International Conference on Robotics and Automation (ICRA)*, pages 5846–5851. IEEE, 2015.

[12] Zhi Ern Teoh, Sawyer B Fuller, Pakpong Chirarattananon, NO Prez-Arancibia, Jack D Greenberg, and Robert J Wood. A hovering flapping-wing microrobot with altitude control and passive upright stability. In *2012 IEEE/RSJ International Conference on Intelligent Robots and Systems*, pages 3209–3216. IEEE, 2012.

[13] Diana A Olejnik, Bardienus P Duisterhof, Matej Karásek, Kirk YW Scheper, Tom Van Dijk, and Guido CHE De Croon. A tailless flapping wing mav performing monocular visual servoing tasks. *Unmanned Systems*, 8(04):287–294, 2020.

[14] IC Cheeseman and WE Bennett. The effect of the ground on a helicopter rotor. *R & M*, 3021, 1957.

[15] Sanjukta Aich, Chahat Ahuja, Tushar Gupta, and P Arulmozhivarman. Analysis of ground effect on multi-rotors. In *2014 International Conference on Electronics, Communication and Computational Engineering (ICECCE)*, pages 236–241. IEEE, 2014.

[16] Yuan Xu, Yuriy S Shmaliy, Xiyuan Chen, Yueyang Li, and Wanfeng Ma. Robust inertial navigation system/ultra wide band integrated indoor quadrotor localization employing adaptive interacting multiple model-unbiased finite impulse response/kalman filter estimator. *Aerospace Science and Technology*, 98:105683, 2020.

[17] Steven van der Helm, Mario Coppola, Kimberly N McGuire, and Guido CHE de Croon. On-board range-based relative localization for micro air vehicles in indoor leader–follower flight. *Autonomous Robots*, 44(3):415–441, 2020.

[18] Matěj Karásek, Mustafa Percin, Torbjørn Cunis, Bas W van Oudheusden, Christophe De Wagter, Bart DW Remes, and Guido CHE de Croon. Accurate position control of a flapping-wing robot enabling free-flight flow visualisation in a wind tunnel. *International Journal of Micro Air Vehicles*, 11:1756829319833683, 2019.

[19] Matej Karasek. Flapper drones. https://flapper-drones.com/wp/. Accessed: 2021-01-01.

[20] Controllers in the crazyflie. https://www.bitcraze.io/documentation/repository/crazyflie-firmware/2020.04/functional-areas/controllers/. Accessed:2021-02-01.

[21] Mark W Mueller, Michael Hamer, and Raffaello D'Andrea. Fusing ultra-wideband range measurements with accelerometers and rate gyroscopes for quadrocopter state estimation. In *2015 IEEE International Conference on Robotics and Automation (ICRA)*, pages 1730–1736, May 2015.

[22] Matěj Karásek, Florian T Muijres, Christophe De Wagter, Bart DW Remes, and Guido CHE de Croon. A tailless aerial robotic flapper reveals that flies use torque coupling in rapid banked turns. *Science*, 361(6407):1089–1094, 2018.

[23] Taimur Ali Shams, Syed Irtiza Ali Shah, Ali Javed, and Syed Hossein Raza Hamdani. Airfoil selection procedure, wind tunnel experimentation and implementation of 6dof modeling on a flying wing micro aerial vehicle. *Micromachines*, 11(6):553, 2020.

[24] Li Danjun, Zhou Yan, Shi Zongying, and Lu Geng. Autonomous landing of quadrotor based on ground effect modelling. In *2015 34th Chinese Control Conference (CCC)*, pages 5647–5652. IEEE, 2015.